Microgravity Science and Technology (2023) 35:6
https://doi.org/10.1007/s12217-023-10036-1

RESEARCH

Zero-Offset Analysis on Differential Wavefront Sensing Technique in Gravitational Wave Detection Missions

Ruihong Gao[1] · Yikun Wang[4,5,6] · Zhao Cui[4,5] · Heshan Liu[1] · Jianjun Jia[3,4,5,6] · Ziren Luo[1] · Gang Jin[2]

Received: 20 May 2022 / Accepted: 16 January 2023 / Published online: 3 February 2023

Abstract

Benefiting from ultra-high angular resolution, differential wavefront sensing (DWS) technique is widely used in gravitational wave detection missions for suppressing the laser pointing jitter as well as sensing jitter of the test mass. However, the zero-offset property of the DWS which leads to absolute angular measurement error is rarely mentioned in previous researches. In this paper, we describe the mechanisms causing the DWS zero-offset with an analytical model as well as numerical method. With the analytical results, we analyze the static pointing error of the gravitational wave detection satellite induced by the DWS. As the error is far larger than the requirement of 10 nrad magnitude, a zero-offset reduction scheme is proposed. We also construct an experiment system for verifying the theoretical results. The experimental results show that the DWS zero-offset can be effectively suppressed with the proposed scheme.

Keywords Differential wavefront sensing · Laser pointing · Gravitational waves detection

Introduction

LISA (Laser Interferometer Space Antenna) Danzmann and Rüdiger (2003), Taiji Luo et al. (2020), Hu and Wu (2017), Luo et al. (2021) are the most representative space-based gravitational wave detection missions aiming at signals in the frequency band from 0.1 mHz to 1 Hz. Compared with the ground-based programs, an inter-satellite laser link constellation has to be constructed before science measurement. Because of the imperfect telescope, the satellite jitter caused by complex space environment will cause laser pointing jitter noise even with a dedicated drag free system. For achieving arm-length variations measurement of picometer precision, the laser pointing jitter need to be suppressed to 10 $\mathrm{nrad}/\sqrt{\mathrm{Hz}}$ (1 mHz-1 Hz) Bender (2005). Traditional angular measurement methods can hardly fulfill the requirement.

Differential wavefront sensing (DWS) technique provides an effective method for precision angular measurement in

Ruihong Gao and Yikun Wang have contributed equally.

✉ Ziren Luo
luoziren@imech.ac.cn

✉ Gang Jin
gajin@imech.ac.cn

Ruihong Gao
gaoruihong@ucas.ac.cn

Yikun Wang
wangyikun@ucas.ac.cn

Zhao Cui
cz447047276@163.com

Heshan Liu
liuheshan@imech.ac.cn

Jianjun Jia
jjjun10@mail.sitp.ac.cn

[1] Center for Gravitational Wave Experiment, National Microgravity Laboratory, Institute of Mechanics, Chinese Academy of Sciences, Beijing 100190, China

[2] School of Fundamental Physics and Mathematical Sciences, Hangzhou Institute for Advanced Study, UCAS, Hangzhou 310024, China

[3] University of Chinese Academy of Sciences, Beijing 100049, China

[4] Key Laboratory of Gravitational Wave Precision Measurement of Zhejiang Province, Hangzhou Institute for Advanced Study, UCAS, Hangzhou 310042, China

[5] School of Physics and Optoelectronic Engineering, Hangzhou Institute for Advanced Study, UCAS, Hangzhou 310024, China

[6] Key Laboratory of Space Active Opto-Electronics Technology, Shanghai Institute of Technical Physics, Chinese Academy of Sciences, Shanghai 200083, China

laser interferometers Morrison et al. (1994a, b). The DWS signal can be generated from the phase difference between different quadrants of the quadrant photo diode (QPD), which can be written as,

$$DWS_{rl} = \frac{\varphi_1 + \varphi_4 - \varphi_2 - \varphi_3}{2}, \quad DWS_{ud} = \frac{\varphi_1 + \varphi_2 - \varphi_3 - \varphi_4}{2}, \tag{1}$$

where, $\varphi_1, \varphi_2, \varphi_3, \varphi_4$ are the phase of the interference signal of each quadrant. The DWS signal is approximately proportional to the angle between two interfering beams. Benefiting from high achievable phase measurement sensitivity and great common mode rejection effect, nano-radian angular resolution can be obtained Dong et al. (2014). As a result, the DWS technique is the preferred solution for the laser pointing system as well as the test-mass attitude monitor of LISA and Taiji Heinzel (2004).

So far, a considerable amount of literature has been published on the DWS. The linearity performance of the technique is well discussed with ideally derived analytical expressions Hechenblaikner (2010). Moreover, the impact of beam property, aberration and alignment to the linearity range has also been focused on based on numerical method Yu et al. (2015). Obviously, the non-linearity characteristic decreases the angular resolution of the DWS. As a result, the linearity range, to a great extent, dominates the jitter attenuation level of the laser pointing system. Methodological demonstration experiments are also carried out on ground as well as on the LISA Pathfinder satellite Lennart et al. (2017) for verifying the feasibility of the technique.

However, taking LISA as an example, for decreasing the laser pointing jitter noise, the static pointing error should also be suppressed to 10 nrad besides pointing jitter Bender (2005). Traditionally, assembly error between the optical bench and the telescope is considered to be the major contributor. The attitude of the satellite, which is adjusted based on the DWS read out, actually influences the direction of both the transmitting and the receiving optical axis. Thus, the absolute angular measurement error of the DWS will induce additional static pointing error. Ideally, the receiving beam is considered parallel with the local beam when the DWS signal equals to zero. However, residual angle between the interfering beams may exist with zero DWS value, which can be described as the zero-offset property. The absolute angular measurement accuracy is mainly determined by the offset value. To our best knowledge, there has been little quantitative analysis of this topic. Only Enrico Massa Massa et al. (2019) mentioned that mismatches and aberrations may induce fake tilt of the DWS. Further researches is still needed to quantify the influence of the zero-offset to the laser pointing system.

In this paper, we describe the mechanisms causing the DWS zero-offset property. In "Analytical Expression of DWS Zero-offset Value", we firstly derive the analytical expression of the zero-offset with the model of practical application. In "Numerical Results and Discussion", numerical method is introduced to verify the analytical expressions. With the theoretical results, we calculate the static pointing error induced by the DWS and propose an approach to suppress the offset value. In "Experimental Results", an experiment is also carried out for verifying the theoretical results and the zero-offset reduction scheme, followed by a summary in "Conclusion".

Analytical Expression of DWS Zero-offset Value

We start by deriving the analytical expression of the zero-offset value in practical application with the model illustrated in Fig. 1. Where, (x_Q, y_Q, z_Q) is the QPD coordinate, (x_0, y_0) is the emission coordinate of two beams. In order to improve the common mode rejection performance of the interferometer, both the local and the receiving beams are designed to propagate the same distance s on the optical bench. The alignment errors and the flat top feature of the receiving beam, which are usually ignored in previous researches, are considered here. For simplifying calculation, a square QPD is assumed and the influence of aberration is ignored. Moreover, only the alignment errors in the horizontal direction are taken into account. Because of the symmetric distribution of the wavefront in the top and bottom quadrants, the offset of the beams will only influence the DWS signal of left and right quadrants. Same conclusions can also be obtained with the beam offset in the vertical direction.

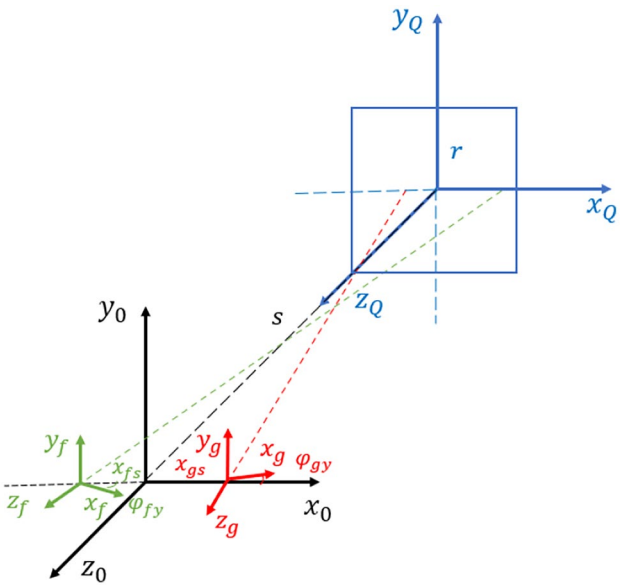

Fig. 1 Coordinate systems of the interferometer. Where, (x_Q, y_Q, z_Q) is the QPD coordinate, (x_0, y_0, z_0) is the emission coordinate of two beams, s is the beam propagation distance, (x_{gs}, φ_{gy}) denotes the position and angular offset of the local Gaussian beam, (x_{fs}, φ_{fy}) denotes the position and angular offset of the receiving flat top beam and r is the half length of the QPD

In local laser coordinate (x_g, y_g, z_g), the Gaussian beam can be expressed as,

$$E_g = A_g \cdot exp(-\frac{x_g^2 + y_g^2}{\omega_z^2}) exp(-ik(\frac{x_g^2 + y_g^2}{2R_z} - z_g)). \tag{2}$$

With the waist radius denoted as ω_0, the beam size ω_z and the wavefront curvature radius R_z can be written as,

$$\omega_z = \omega_0 \sqrt{1 + (z/z_R)^2}, \qquad R_z = z[1 + (z_R/z)^2], \tag{3}$$

where, $z_R = \pi\omega_0^2/\lambda$ is the Rayleigh distance.

After a few million kilometers propagation, the receiving beam clipped by the telescope has the properties of a flat top beam, whose coordinate is denoted as (x_f, y_f, z_f). Assuming that the size of flat top beam is far larger than the QPD, we can write the flat top beam as,

$$E_f = A_f \cdot exp(-ik(-z_f)). \tag{4}$$

In practical applications, alignment errors including beam center mismatch and beam tilt can not be ignored. We define x_{gs}/x_{fs} and $\varphi_{gy}/\varphi_{fy}$ as the position and angular offset of the Gaussian and the flat top beam generated from alignment errors. Hence, the complex amplitude of the beams on the QPD $E_g^{'}/E_f^{'}$ can be obtained with the transformation formula,

$$\begin{pmatrix} x_{is} \\ y_{is} \\ z_{is} \end{pmatrix} = \begin{pmatrix} cos\varphi_{iy} & 0 & sin\varphi_{iy} \\ 0 & 1 & 0 \\ -sin\varphi_{iy} & 0 & cos\varphi_{iy} \end{pmatrix} \begin{pmatrix} x_Q - x_{is} \\ y_Q \\ z_Q - s \end{pmatrix}, \tag{5}$$

where, i can be replaced by g or f.

Then, the interference pattern on the right and left half of the QPD can be respectively denoted as,

$$F_{right} = \int_{-r}^{r}\int_{0}^{r} E_g^{'} E_f^{'*} dx_Q dy_Q, \quad F_{left} = \int_{-r}^{r}\int_{-r}^{0} E_g^{'} E_f^{'*} dx_Q dy_Q. \tag{6}$$

Thus, the DWS signal in the horizontal direction can be written as,

$$DWS_{rl} = arg(F_{right}) - arg(F_{left}) = arg(\frac{F_{right}}{F_{left}}). \tag{7}$$

As beam offset values are of 10 μm/10 μrad magnitude after calibration, both the two beams propagate approximately the same distance, that is $z_g = z_f = s$. After substituting formulas (2)-(6) into (7), we can achieve that

$$DWS_{rl} = arg\{\frac{erf\, i[\sqrt{C_1}(r + \frac{C_2}{2C_1})] - erf\, i(\frac{C_2}{2\sqrt{C_1}})}{erf\, i[\sqrt{C_1}(r - \frac{C_2}{2C_1})] + erf\, i(\frac{C_2}{2\sqrt{C_1}})}\}. \tag{8}$$

where,

$$C_1 = -(\frac{ik}{2R_z} + \frac{1}{w_z^2}), \tag{9}$$

$$C_2 = \frac{2(x_{gs} + s\varphi_{gy})}{\omega_z^2} + ik(\frac{x_{gs} + s\varphi_{gy}}{R_z} + \varphi_{fy} - \varphi_{gy}). \tag{10}$$

As the offset values x_{is} and φ_{iy} are small enough, $\frac{C_2}{2C_1}$ approximately equals to zero. On the other hand, $\frac{1}{w_z^2} \gg \frac{k}{2R_z}$ in most cases. Therefore,

$$erf\, i[\sqrt{C_1}(r + \frac{C_2}{2C_1})] \approx erf\, i[\sqrt{C_1}(r - \frac{C_2}{2C_1})] \approx i \cdot erf(\frac{r}{w_z}). \tag{11}$$

We neglect terms of second order or higher of x_{is}, φ_{iy} as well as any cross-terms. After expansion of the error function to first order, we can also get,

$$erf\, i[\frac{C_2}{2\sqrt{C_1}}] \approx \frac{C_2}{\sqrt{\pi C_1}}. \tag{12}$$

Make $\delta = k\omega_z^2/2R_z$, then

$$\frac{1}{\sqrt{\pi C_1}} = \frac{-i\omega_z}{\sqrt{\pi}} \sqrt{\frac{1 - i\delta}{1 + \delta^2}}. \tag{13}$$

We make $\varphi_i = \varphi_{fy} - \varphi_{gy}$ denote the included angle of two interfering beams. Assuming the alignment errors are much smaller than φ_i, it can be given that,

$$\frac{C_2}{\sqrt{\pi C_1}} \approx k\omega_z[\frac{x_{gs}}{R_z} + (\frac{s}{R_z} - 1)\varphi_{gy} + \varphi_{fy}] \sqrt{\frac{1 - i\delta}{1 + \delta^2}}. \tag{14}$$

Then, we substitute formulas (11) and (14) into (8). Thus,

$$DWS_{rl} \approx arg(1 + i\frac{2\xi}{\sqrt{\pi} erf(\frac{r}{\omega_z})}). \tag{15}$$

After expanding the formula (15) to first order in x_{is} and φ_{iy}, we find

$$DWS_{rl} \approx C_3(\varphi_i + \Delta\varphi) + O(x_{is}^2, \varphi_{iy}^2), \tag{16}$$

where

$$C_3 = \frac{k\omega_z}{erf(\frac{r}{\omega_z})} \sqrt{\frac{2}{\pi} \frac{1 + \sqrt{1 + \delta^2}}{1 + \delta^2}}, \tag{17}$$

$$\Delta\varphi = \frac{x_{gs} + s\varphi_{gy}}{R_z}. \tag{18}$$

Traditionally, the non-linearity of the DWS denoted as $O(x_{is}^2, \varphi_{iy}^2)$ is regarded as the major contributor to the angular measurement error. However, from formula (16) it can be found that an additional zero-offset error is induced by the factor $\Delta\varphi$. That is to say, the included angle of two beams will be controlled to a nonzero value $-\Delta\varphi$ based on the DWS technique. We can also learn from formula (18) that the zero-offset actually comes from the beam alignment errors and its value increases linearly with the increase of the local Gaussian beam alignment errors. As a large receiving flat top beam is assumed, its alignment error will not appear in the zero-offset factor.

Numerical Results and Discussion

To verify the validity of the above analytical results, we adopt numerical method. We first build an interferometer model as illustrated in Fig. 1 with practical beam features based on the MATLAB platform. Then, the phase of the heterodyne signal within the four quadrants of the QPD is obtained by calculating the argument of the interference signal. With the help of formula (1), we can get the numerical results of the DWS. Compared with the analytical derivation, the ignored high-order terms in x_{is} and φ_{iy} are taken into account here. On the other hand, a circular QPD which is usually used in practical applications replaces the square one.

With $s = 2$ m, $r = 0.6$ mm, $\omega_0 = 0.5$ mm, we firstly assume that there is only angular alignment error of the Gaussian beam, that is $x_{gs} = 0$. Figure 2(a) presents numerical results of the relationship between the included angle φ_i and the corresponding DWS signal with various φ_{gy} values. It can be found that the zero-offset apparently exists. We record the offset $\Delta\varphi$ as the φ_i value when DWS equals to zero. Then, we can draw the relation curve of φ_{gy} and $\Delta\varphi$ as illustrated in Fig. 2(b). With the help of formula (18), analytical results are also presented in the same figure. After comparison, it can be found that the numerical and analytical results matches very well.

Then, we assume that there is only translation offset of the Gaussian beam. Figure 3(a) and (b) present the DWS signal and $\Delta\varphi$ with different x_{gs}. It comes to the same conclusion. Thus, the square QPD assumption in "Analytical Expression of DWS Zero-Offset Value" has little impact. The slight deviation mainly comes from the first order approximation we made in the analytical derivation. Therefore, it is reasonable to estimate the zero-offset value with formula (18).

Then, we try to estimate the static pointing error caused by the DWS. Taking the Taiji program as an example, a static pointing error of 10 nrad is required. With the 400× magnification of the telescope and the imaging system, the pointing precision at the QPD should reach 4 μrad. As a result, the zero-offset value of the DWS should be smaller than 0.4 μrad after considering some redundancy. With the best achievable alignment level, the Gaussian beam offset can be limited to $x_{gs} = 10\,\mu$m, $\varphi_{gy} = 10\,\mu$rad. After substituting the above system parameters into formula (18), $\Delta\varphi$ is calculated as large as 13.2 μrad, which is far larger than the requirement. Therefore, a zero-offset reduction scheme must be considered.

From formula (18), it can be found that $\Delta\varphi$ is in reverse proportion to the Gaussian beam radius curvature R_z. If R_z tends to infinite, which can be fulfilled at the beam waist position, the zero-offset is eliminated in theory. Therefore, we propose to adopt a dedicated imaging system and place the QPD on the conjugate plane of the waist position. As given in the formula (3), R_z is a function of the beam propagation distance from the beam waist position. Thus, Fig. 4 presents the relationship between s and $\Delta\varphi$. We can draw the conclusion that $\Delta\varphi$ decreases with the decrease of s. Moreover, $\Delta\varphi$ can meet the static laser pointing requirement of Taiji when the beam waist propagation distance is smaller than 2 cm. The requirement can be easily fulfilled after assembling the imaging system as well as calibrating the waist position.

Experimental Results

We have learned from formula (18) and the numerical results that $\Delta\varphi$ is proportion to x_{gs} and φ_{gy} and inversely proportion to R_z. If we can image the beam waist to the QPD surface, the zero-offset can be eliminated theoretically. For further verifying the conclusions, an experimental system is constructed.

Experimental Setup

The experimental setup is illustrated in Fig. 5. The receiving flat top beam from FC1 is simulated by a 20× beam expander and an aperture of 1.2 mm radius. As the radius of the QPD is 0.6 mm, the size of the receiving beam is far larger than the QPD size, which is consistent with the assumption in "Analytical Expression of DWS Zero-offset Value". The local Gaussian beam whose waist radius is 0.5 mm is transmitted from FC2. Two acousto optic modulators (AOMs) are used to generate the heterodyne signal of 1.6 MHz beat frequency. FSM1 and FSM2 are two fast steering mirrors driven by PI S-330 piezo actuator, whose angular resolution is 0.02 μrad. The FSMs are used to change the angle of the interference beams. Lens2 is an afocal imaging system making the rotation center of FSM1/FSM2 and the QPD position form a conjugate plane pair. It can not only eliminate the influence of beam walk to the DWS, but also examine the performance of the zero-offset reduction scheme. For keeping the flat top feature of the receiving beam, Lens1 is used to eliminate the diffraction effect by imaging the aperture center to the rotation center of FSM1.

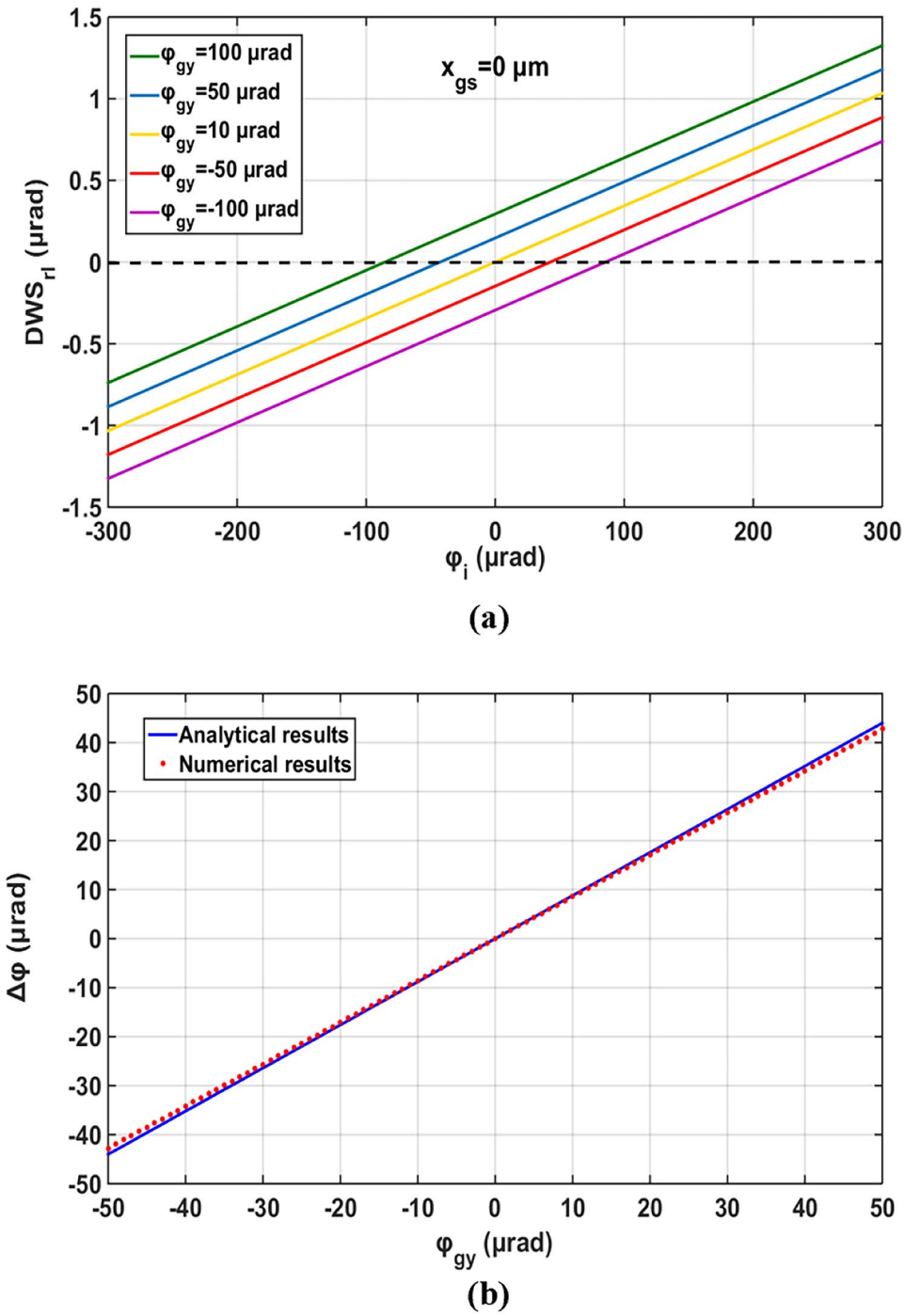

Fig. 2 **a** The relationship between the included angle and the corresponding DWS signal. Where, $x_{gs} = 0$ μm and φ_{gy} various from -100 μrad to 100 μrad. **b** Comparison between the analytical results and the numerical results of the zero-offset with different φ_{gy}

Phasemeter calculates the DWS signal based on the interference signal detected by the QPD.

In order to examine the zero-offset value, we need to measure the absolute angle between two interfering beams to sub-μrad magnitude. Thus, a collimator combined with a beam profiler are introduced in the experiment. The structure of the measurement system is illustrated in the right part of Fig. 5. Both of the two beams enter the entrance of the collimator and reflected by a concave mirror whose focal length is $f = 4$ m. The beam profiler is a CCD camera. It is sited at the focal plane of the concave mirror. Then, the included angle can be calculated as $\Delta\varphi = f\Delta x$, where Δx denotes the distance between two laser spots on the CCD surface. With a dedicated centroid method Gao et al. (2020), the spot center positioning precision is better than 0.1 pixel. As the pixel size of the profiler is 5 μm, the corresponding measurement accuracy of Δx is 0.5 μm. Therefore, the angular measurement precision is 0.125 μrad theoretically. After considering some

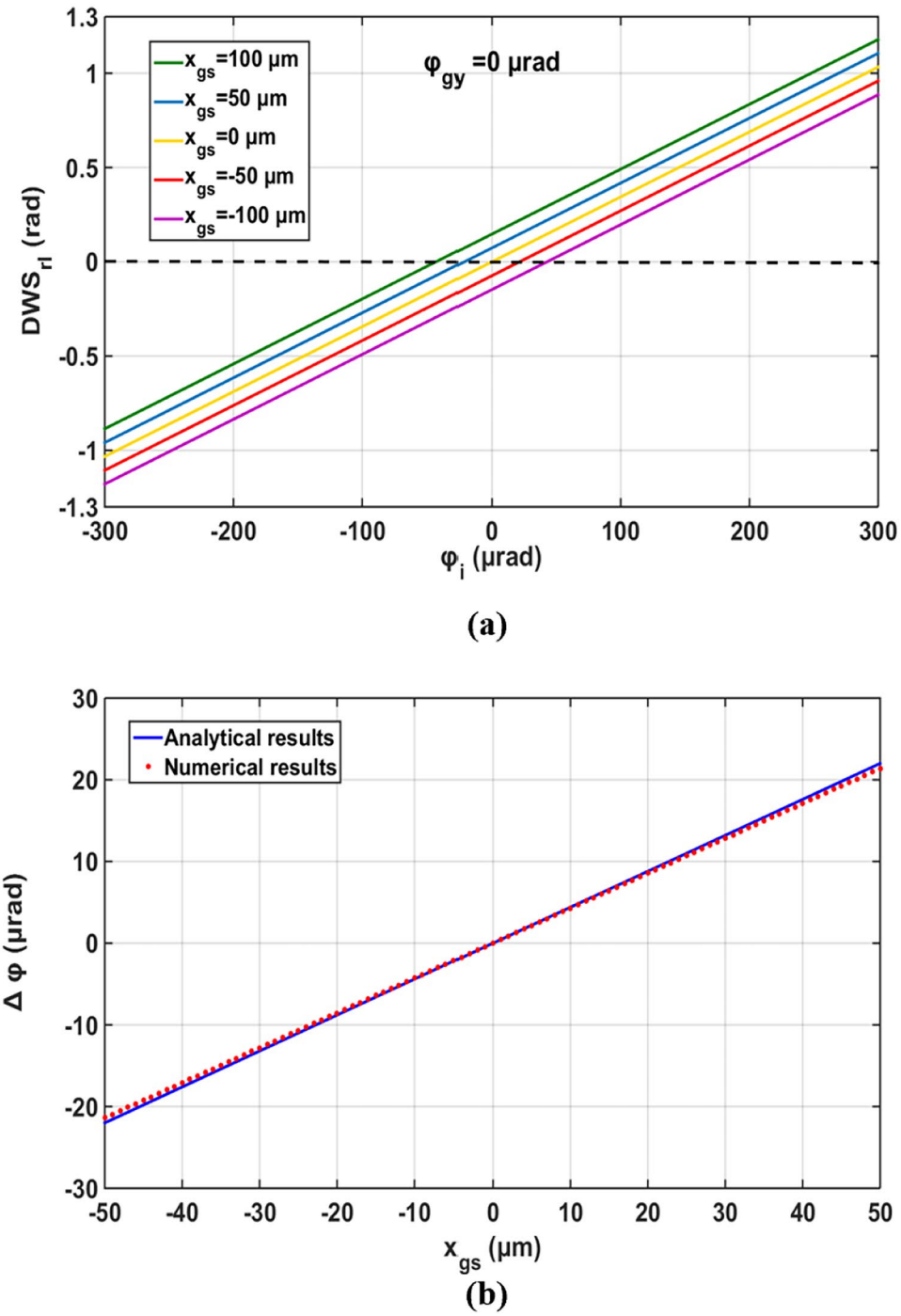

Fig. 3 **a** The relationship between the included angle and the corresponding DWS signal. Where, $\varphi_{gy} = 0\ \mu$rad and x_{gs} various from $-100\ \mu$m to $100\ \mu$m. **b** Comparison between the analytical results and the numerical results of the zero-offset with different x_{gs}

redundancy, the readout precision of the collimator system is evaluated as $\phi_{col} = 0.5\ \mu$rad. Moreover, the measurement accuracy of the experimental system is also influenced by the readout precision of the DWS under atmosphere environment ϕ_{DWS} and the ground vibration ϕ_{vib} because the optical system and the collimator system are placed on different tables. As a result, the measurement accuracy of the experimental system can be calculated as $\phi_{exp} = \sqrt{\phi_{col}^2 + \phi_{DWS}^2 + \phi_{vib}^2}$. ϕ_{exp} is evaluated as 1 μrad magnitude, which is enough for the verification experiment.

Verification of the Relationship Between Zero-offset and Lateral Alignment Error

We firstly study the influence of x_{gs} to $\Delta\varphi$ with the experimental system. The position without beam offset can hardly be determined exactly. However, the linearity

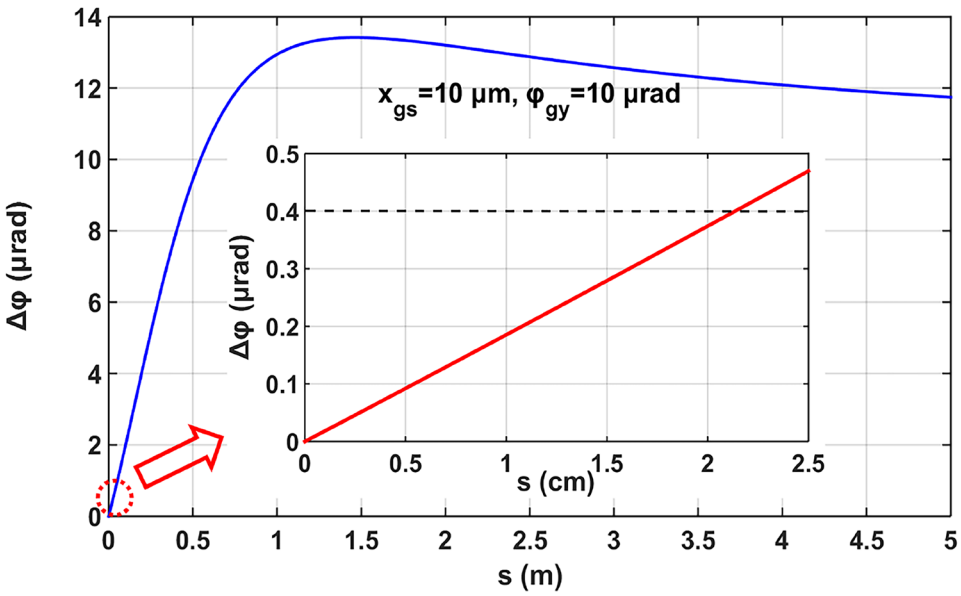

Fig. 4 The relationship between the beam waist propagation distance and the zero-offset value. Where, $s = 2$ m, $r = 0.6$ mm, $\omega_0 = 0.5$ mm, $x_{gs} = 10$ μm and $\varphi_{gy} = 10$ μrad

performance can still be verified with the variation of x_{gs} and the variation of $\Delta\varphi$. As the flat top beam radius is far larger than the QPD size, the QPD position variation x_s is equivalent to the Gaussian beam position offset x_{gs}. For shifting the relative position conveniently, the QPD is placed on an one-dimensional precision translation stage. For each QPD position, the attitude of FSM1 is adjusted to make the DWS signal equals to zero, while FSM2 stays still. Then, the included angle of the two interference beams is read out by the collimator system as φ_e. Here, φ_e is the estimation of $\Delta\varphi$. To verify the zero-offset reduction scheme, we carry out the process with the beam waist of the Gaussian beam near and far from FSM2 center respectively. The nominal value of the waist position is about 200 mm from the fiber coupler head. We check the value by searching for the position with the least spot size with the help of a beam profiler. As the QPD is placed on the conjugate plane of FSM2 rotation center, the zero-offset can be theoretically eliminated when the beam waist is near FSM2 center. As illustrated in Fig. 6, data1 and data2 presents the experimental results of the relationship between the position offset and the DWS zero-offset value. The yellow line and the green line are the corresponding linear fitting curves.

It can be found that φ_e has good linear relationship with x_s. It is consistent with the theoretical results. The root mean square error (RMSE) value are introduced to evaluate the deviation between experimental data and related linear fitting results. The RMSE value of data1 and data2 are calculated as 9.8 μrad and 2.3 μrad. Therefore, the small deviation

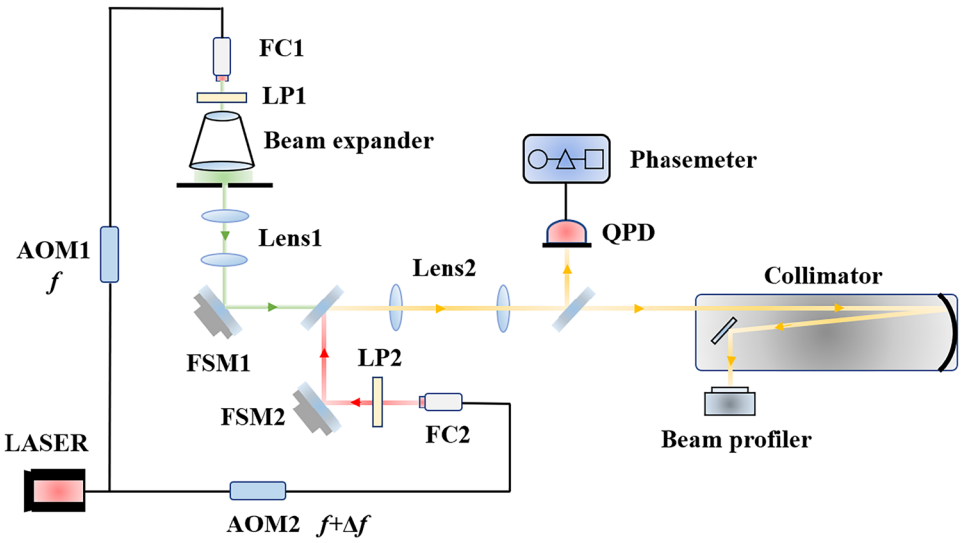

Fig. 5 Diagram of the experimental system for verifying the zero-offset reduction scheme. Where, FC is the fiber collimator, LP is the linear polarizer, FSM is the fast steering mirror

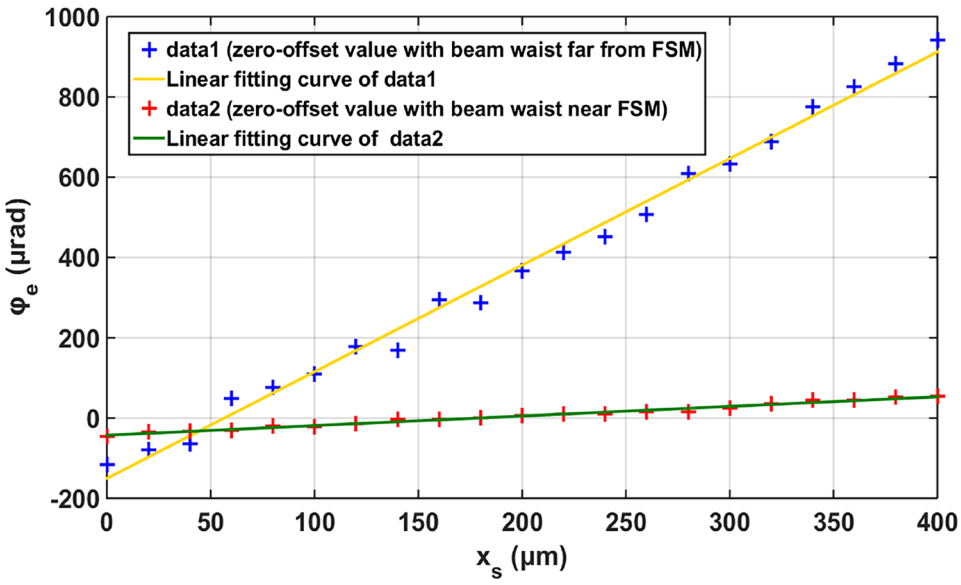

Fig. 6 The experimental results of DWS zero-offset value with various QPD position offset. Where, data1 is recorded when the Gaussian beam waist is far from FSM2, data2 is recorded when the beam waist is near FSM2. The yellow and green line are the corresponding linear fitting curves

mainly comes from the angular measurement error of the experimental system. As x_s denotes the variation of the QPD position rather than the exact value of x_{gs}, the linear fitting curves do not pass through the origin. By comparing data1 with data2, we can find that the slope of the green linear fitting curve is far less than the yellow one. That is to say, the DWS zero-offset induced by the beam position offset can be effectively suppressed when the QPD is placed on the conjugate plane of the waist position. However, there is slight uplift of the green curve. This is mainly because both the position offset of the local beam and the receiving beam are changed when the QPD position is shifted. Theoretically, the flat top beam position offset has no impact on $\Delta\varphi$. However, small truncation ratio and residual diffraction in the experiment make the receiving beam a non-ideal flat top beam.

Verification of the Relationship Between Zero-offset and Angular Alignment Error

In the next step, we pay attention to the Gaussian beam angular offset, which can be easily changed with the help of FSM2. FSM2 angular variation is denoted as φ_s. It is half of the variation of φ_{gy}. For each angle of FSM2, the attitude of FSM1 is adjusted to make the DWS signal equals to zero, while the QPD position stays still. The zero-offset value is also estimated by φ_e. Similarly, the process is repeated twice with the local beam waist near and far from FSM2 respectively. The experimental results are shown in Fig. 7.

It can be found that the zero-offset value has good linear relationship with the beam angular offset. The RMSE value of data1 and data2 are calculated as 5.8 μrad and 7.6 μrad.

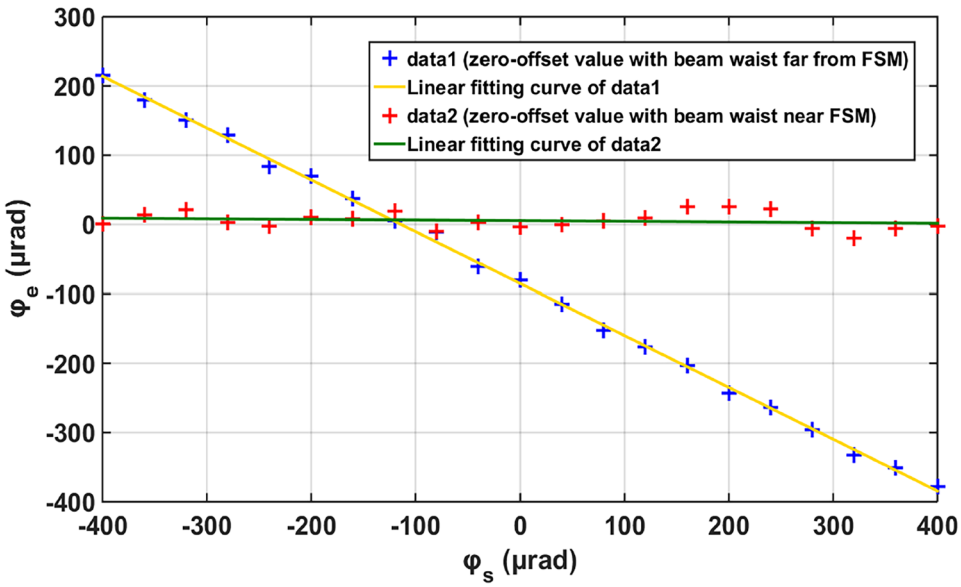

Fig. 7 The experimental results of DWS zero-offset value with various FSM2 angular offset. Where, data1 is recorded when the Gaussian beam waist is far from FSM2, data2 is recorded when the beam waist is near FSM2. The yellow and green line are the corresponding linear fitting curves

The angular measurement error of the experimental system is also the main contributor. Therefore, the theoretical results are further verified. Moreover, as only the angle of the local beam is shifted this time, the non-flat top properties have little impact on the results. As a result, the slope of the green curve is very close to zero. Therefore, it is apparent that the DWS zero-offset induced by the φ_{gy} can also be effectively suppressed with the proposed scheme.

Conclusion

This paper has provided a deeper insight into the DWS technique. We analyse the DWS zero-offset property, which is ignored in previous researches. Zero-offset will decrease the absolute angular measurement precision rather than the angular resolution. The latter one is mainly influenced by the non-linearity property. We firstly describe the mechanisms causing the DWS zero-offset with an analytical model. The analytical results indicate that the zero-offset mainly comes from the alignment errors of the local Gaussian beam, and the offset value increases linearly with increase of the alignment errors. The correctness of analytical results is verified by the numerical method. Then we study the static pointing error induced by the DWS zero-offset in LISA-like programs with the analytical expression. Even with the best achievable alignment level, the zero-offset value is still as large as 10 μrad magnitude, which is far beyond the requirement. As a result, we propose to adopt a dedicated imaging system and place the QPD on the conjugate plane of the waist position. Theoretically, the zero-offset can be eliminated with the scheme. We build an experimental system for verification. The experimental results are well coincident with the theory, while the zero-offset reduction scheme is fully validated. The results we obtained here will improve the absolute angular measurement precision in future laser pointing systems.

Acknowledgements The authors would like to thank the National Key R &D Program of China (2020YFC2200104), and the Strategic Priority Research Program of the Chinese Academy of Sciences (Project No. XDA1502110102, No. XDA1502110103) for the financial support.

Author Contributions Ruihong Gao and Yikun Wang wrote the main manuscript text. Zhao Cui, Heshan Liu and Jianjun Jia provided technique support in manuscript preparation. Ziren Luo and Gang Jin provided the innovation of the manuscript. All authors reviewed the manuscript.

Funding This study was supported in part by grants from The National Key R &D Program of China (2020YFC2200104), and the Strategic Priority Research Program of the Chinese Academy of Sciences (Project No. XDA1502110102, No. XDA1502110103).

Data Availability The data that support the findings of this study are available from the corresponding author upon reasonable request.

Declarations

Ethics Approval Not applicable.

Consent to Participate Not applicable.

Consent for Publication Not applicable.

Conflicts of Interest The authors declare that they have no conflicts of interests.

References

Bender, P.L.: Wavefront distortion, and beam pointing for LISA. Class. Quant. Grav. **22**, 339 (2005)
Danzmann, K., Rüdiger, A.: LISA technology-concept, status, prospects. Class. Quant. Grav. **20**, s1 (2003)
Dong, Y.-H., Liu, H.-S., Luo, Z.-R., Li, Y.-Q., Jin, G.: Methodological demonstration of laser beam pointing control for space gravitational wave detection missions Rev. Sci. Instr **85**, 0745041 (2014)
Gao, R.-H., Liu, H.-S., Zhao, Y., Luo, Z.-R., Jin, G.: A high precision laser spot center positioning method for weak light conditions. Appl. Opt. **59**, 1763 (2020)
Hechenblaikner, G.: Measurement of the absolute wavefront curvature radius in a heterodyne interferometer. Opt. Soc. Am. A. **27**, 2078 (2010)
Heinzel, G., et al.: The LTP interferometer and phasemeter Class. Quant. Grav. **21**, S581 (2004)
Hu, W.-R., Wu, Y.L.: Taiji program in space for gravitational wave physics and nature of gravity. Natl. Sci. Rev. (2017)
Lennart, W., et al: LISA Pathfinder: Understanding DWS noise performance for the LISA mission. J. Phys.: Conf. Ser. **840**, 012044 (2017)
Luo, Z.-R., Guo, Z.-K., Jin, G., Wu, Y.L., Hu, W.R.: A brief analysis to Taiji: Science and technology. Results. Phys. **16**, 102918 (2020)
Luo, Z.-R., Wang, Y., Wu, Y.L., Hu, W.R., Jin, G.: The Taiji program: A concise overview. Prog. Theor. Exp. Phys. **5**, 05A108 (2021)
Massa, E., Sasso, C.P., Mana, G.: Fake tilts in differential wavefront sensing. Opt. Exp. **27**, 34505 (2019)
Morrison, E., Robertson, B., Ward, H.: Experimental demonstration of an automatic alignment system for optical interferometers. Appl. Opt. **33**, 5037–5040 (1994a)
Morrison, E., Robertson, B., Ward, H.: Automatic alignment of optical interferometers. Appl. Opt. **33**, 5041–5049 (1994b)
Yu, X.-Z., Gillmer, S.R., Ellis, J.D.: Beam geometry, alignment, and wavefront aberration effects on interferometric differential wavefront sensing. Meas. Sci. Technol. **26**, 125203 (2015)